Chinese Journal of Chemical Engineering 89 (2026) 1–12

Contents lists available at ScienceDirect

Chinese Journal of Chemical Engineering

journal homepage: www.elsevier.com/locate/CJChE

Full Length Article

Efficient leukocyte removal and enhanced biocompatibility using PVDF membranes prepared by vapor-induced phase separation

Ziqi Jin [1, 2], Shuang Yao [1, 2], Liang Li [1, 2], Siyuan Sun [1], Yue Zhou [1, 2], Jie Zhou [3], Zhaohui Wang [1, 2], Zhaoliang Cui [1, 2, 3, 4, *]

[1] State Key Laboratory of Materials-Oriented Chemical Engineering, College of Chemical Engineering, Nanjing Tech University, Nanjing 210009, China
[2] National Engineering Research Center for Special Separation Membrane, Nanjing Tech University, Nanjing 210009, China
[3] Jiangsu IKMO Membrane High-Technology Co., Ltd, Suzhou 215300, China
[4] Suzhou Future Membrane Technology Innovation Center, Nanjing Tech University, Suzhou 215300, China

ARTICLE INFO

Article history:
Received 20 May 2025
Received in revised form
14 August 2025
Accepted 15 August 2025
Available online 14 October 2025

Keywords:
Polyvinylidene fluoride membrane
Vapor-induced phase separation
Pore size
Leukocyte filtration
Hemocompatibility

ABSTRACT

To develop an efficient filter for removing white blood cells from whole blood, hydrophilic large-pore blended membranes of poly(vinylidene fluoride) (PVDF), polyvinyl pyrrolidone and polyethylene glycol, with good biocompatibility, were prepared using the process of vapor-induced phase separation at various PVDF concentrations. The results demonstrated that at a PVDF mass concentration of 14%, the membrane had increased surface roughness, significantly enhanced hydrophilicity and wettability, and a wetting time of 8 s. The surface roughness of the membrane was also reduced to 31.637 nm. Furthermore, hemolysis rate and protein adsorption tests indicated that the blended membranes possessed excellent biocompatibility. They were reduced to 2.48% and 34.44 $\mu g \cdot cm^{-2}$, respectively. The pore size of the fabricated membrane was relatively large, which reached approximately 8 μm respectively, satisfying the filtration requirements. Lastly, the effects of different temperatures and multi-layered filters on leukocyte removal and the retention of red blood cells and platelets from whole blood were evaluated. The results revealed that the leukocyte removal rate was highest at 4 °C and with three membrane layers, the leukocyte removal rate was highest, reaching 98.36%, while the RBC and platelet content remained nearly unchanged compared with the original blood. This study provides a new approach for blood cell separation that is expected to play a significant role in medical fields such as blood transfusion demonstrating great potential for application and innovation.

1. Introduction

Blood transfusion is a significant advancement in surgical development and has become a successful approach for rescuing critically ill patients and treating certain diseases. Clinical research data reveals that approximately 1% of blood recipients will experience adverse reactions during the process of receiving blood products for treatment. More than 90% of these adverse reactions are closely associated with white blood cells (WBCs). To stop the occurrence of adverse transfusion reactions, it is necessary to remove WBCs from whole blood as much as possible prior to transfusion [1]. The main methods for leukocyte removal include centrifugation [2], sedimentation [3], washing [4], freezing glycerol removal [5], and filtration [6]. Centrifugation, sedimentation, and washing methods achieve leukocyte removal rates below 85%, while being time-consuming and posing risks of additive residues. Although the frozen glycerol method attains a leukocyte removal rate exceeding 95%, its complex procedure results in low erythrocyte viability and a recovery rate of merely 65%. In contrast, filtration achieves a leukocyte removal rate >99% while maintaining erythrocyte recovery above 85% [7–9]. So the filtration method is generally considered as the most effective way to remove WBCs.

Whole blood filters require a high capacity for removing WBCs while maintaining a high recovery rate for red blood cells (RBCs) and platelets (PLTs). WBC removal is greatly aided by the physical

* Corresponding author. State Key Laboratory of Materials-Oriented Chemical Engineering, College of Chemical Engineering, Nanjing Tech University, Nanjing 210009, China.
E-mail address: zcui@njtech.edu.cn (Z. Cui).

https://doi.org/10.1016/j.cjche.2025.08.017

and chemical characteristics of the filter material, including surface roughness, charge, and contact angle. Unlike WBCs, RBCs lack a nucleus and have a higher deformability. This enables RBCs to pass through smaller pores during filtration, even smaller than their own size. PLTs with a size of 2–3 μm, can easily pass through micropores with a diameter of 3 μm. However, it is difficult for WBCs to pass through pores smaller than 5 μm. Consequently, during filtration, the micropores of 3–8 μm successfully intercept WBCs while allowing RBCs and PLTs to pass through. However, the filtration effectiveness of the filter material can deteriorate or become ineffective if the micropores get clogged by WBCs [10]. The ability of blood cells to pass through the filter material is also influenced by the applied pressure during filtration. When the filter material has smaller pore sizes, withstanding higher pressure is required to facilitate blood flow. However, excessive force on RBCs under high pressure can result in hemolysis, leading to their bursting.

Brui *et al.* [11] found that polyurethane (PU) modified with carboxyl and amine groups exhibited significantly higher WBC adhesion compared with the original polyurethane material. Similarly, Scotchford *et al.* [12] demonstrated that WBC attachment was greater on surfaces coated with polar −COOH and hydrophobic $-CH_3$ monolayer than on those coated with −OH monolayer or monolayer containing ethylene oxide. However, a study by Barbosa *et al.* [13] revealed that the −COOH monolayer had the lowest WBC adhesion when compared with the hydrophobic $-CH_3$ and −OH monolayers. Additionally, Curtis *et al.* [14,15] found that −OH groups on the surface of materials play a crucial role in WBC adhesion. Blocking the −OH groups significantly inhibited WBC attachment, while blocking −COOH did not reduce adhesion to the filter surface. Yang *et al.* [16] conducted an in-depth study on WBC adhesion during blood filtration using poly (butylene terephthalate) non-woven fabric (PBTNF) grafted with various functional groups to control surface wettability. PBTNF made by graft copolymerization of a zwitterionic sulfobetaine, *N*-(3-sulfopropyl)-*N*-methacroyloxyethyl-*N*, *N*-dimethylammonium betaine (SMDB) with a moderate amount of sulfobetaine produced by UV radiation shown greater WBC adhesion, according to their findings. Conversely, PBTNF modified by SMDB and having sulfonic acid groups showed the least amount of adhesion.

Currently, the surface charge of known leukocyte filter materials can be classified into three types: first, those with exclusively negative charges; second, those with both positive and negative charges, but with a net negative charge after balancing; and third, those with both positive and negative charges, but with a net positive charge after balancing. Common negatively charged groups include carboxyl and sulfonic acid groups, while positively charged groups primarily consist of amine, quaternary amine, and *N*-pyrrolidone. Since WBC membranes contain anionic groups like carboxylate and phosphate, their surfaces exhibit a certain degree of electronegativity [17]. This makes WBCs more likely to adhere to positively charged filter materials, while negatively charged filter materials reduce WBC adsorption [18].

Surface wettability is another key factor influencing leukocyte adhesion [19]. Filters with good wettability are more effective at removing WBCs from the blood and can also increase the blood flow rate through the filter. Improved wettability allows blood to pass through the filter more smoothly. Marques *et al.* [20] observed that surfaces with higher hydrophilicity tend to promote greater nucleation and adhesion. However, research by Rodrigues *et al.* [21] showed that increased surface hydrophilicity leads to a reduction in platelet adhesion and activation.

In addition to the materials used in leukocyte removal filters, their manufacturing process is a key factor in determining filtration efficiency. Common leukocyte removal filter membrane preparation methods include electrostatic spinning, vapor-induced phase separation (VIPS) and non-solvent-induced phase separation (NIPS). Among them, VIPS method solves the problem of structural inhomogeneity caused by rapid phase separation in the NIPS method, as well as the risk of low mechanical strength and deep contamination in the electrostatic spinning method, by modulating the vapor mass transfer kinetics. It offers outstanding advantages in precisely controlling the pore size to prevent the formation of a dense epidermal layer and ensuring biocompatibility. By precisely controlling parameters such as temperature and relative humidity, the technology allows fine-tuning of the material structure and properties to meet the specific requirements of different applications, such as membrane distillation [22], bioseparation [23], and anti-pollution filtration [24] at the high end of the spectrum. Poly(vinylidene fluoride) (PVDF) offers excellent processing and mechanical properties, along with a simple preparation process and low cost, making it an ideal material for producing separation membranes [25]. In water treatment, PVDF membranes are frequently utilized, including ultrafiltration [26], microfiltration [27], membrane bioreactors [28,29] and has shown large potential in oil–water separation [30] and biomedical applications [31] in recent years. Venault *et al.* [32] carried out the blood cell separation work using PVDF material, which proved its potential.

The primary objective of this study is to develop a membrane capable of removing WBCs while retaining RBCs and PLTs. The membrane was prepared using the VIPS method. An additive ratio of polyvinyl pyrrolidone (PVP) K90: polyethylene glycol (PEG) 600 at 8:2 was selected to investigate the effect of PVDF concentration on the pore size and properties of the membrane. A blood cell separation system was employed to evaluate the membrane's efficiency, both as a single layer and as a multilayer stack, in removing WBCs and recovering RBCs and PLTs from whole blood.

2. Experimental

2.1. Materials

PVDF (Solef® 6010) was obtained from Solvay Co., Ltd. (Belgium), while PVP K90, *N*,*N*-dimethylacetamide (DMAc), glutaraldehyde, and kerosene were sourced from Shanghai Aladdin Biochemical Technology Co., Ltd., China. PEG 600 was supplied by Beijing Wo Kai Biotechnology Co., Ltd. (China), and the sterile WBC Acrodisc cell filter (commercial membrane) was purchased from PALL Corporation, USA. Bovine serum albumin (BSA) was provided by Anhui Zeseng Technology Co., Ltd., China. Phosphate-buffered saline (PBS) and WBC stain solution were acquired from Beijing Solarbio Science & Technology Co., Ltd. (China), and the bicinchoninic acid (BCA) assay kit was obtained from Shanghai Biyuntian Biotechnology Co., Ltd., China. Whole blood was sourced from Shanghai Yuanye Biotechnology Co., Ltd. (China), while isobutanol and anhydrous ethanol were acquired from Shanghai Lingfeng Chemical Reagent Co., Ltd., China. Saline and purified water were prepared in-house, and the wettability solution (GQ-16) was obtained from Nanjing Gao Qian Functional Materials Co., Ltd., China.

2.2. Preparation of PVDF/PVP/PEG blend membrane

The PVDF leukocyte removal filtration membrane was prepared using the VIPS method, as outlined in Fig. 1. PVDF was weighed at concentrations of 14%, 16%, and 18%, while the amounts of PVP and PEG were kept at concentrations of 8% and 2%. These components were dissolved in DMAc to prepare the casting solution. To guarantee total dissolution, the mixture was put in an oil bath at 60 °C

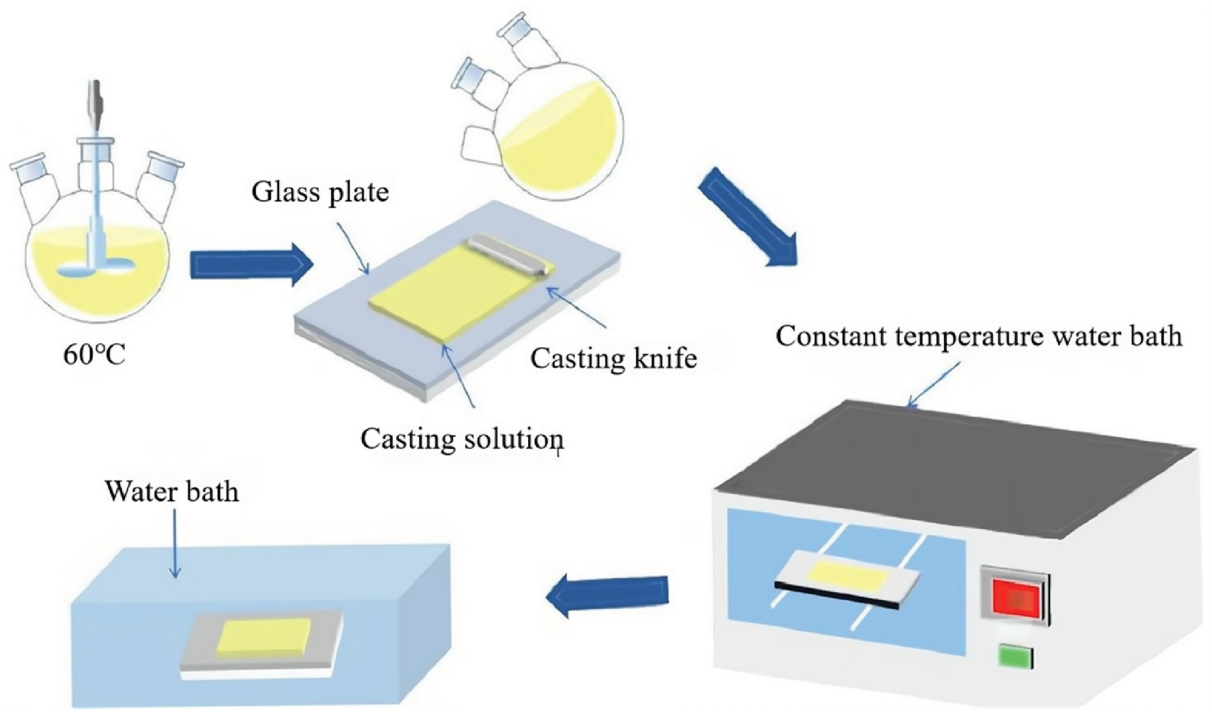

Fig. 1. Schematic diagram of VIPS process for preparing PVDF membrane.

and swirled continuously for 12 h. After stirring, the polymer solution was placed in an oven at 60 °C for 24 h to eliminate any air bubbles formed during the mixing process.

After degassing was finished, a casting knife film applicator was used to evenly apply the polymer solution over a sanitized glass plate (HLKGM3125, Suzhou Sanken Automation Technology Co., Ltd., China, with a gap clearance of 250 μm and casting speed of 1 m·min^{-1}). After that, the glass plate was placed on a pedestal in a water bath that was kept at 60 °C and 60% relative humidity, where solvent exchange was achieved *via* water vapor. After 5 min of water vapor exposure, the plate of glass was set in water bath. Once the membrane separated from the glass plate, it was soaked in pure water for 24 h to remove any residual solvent. After the residual solvent was completely removed, the membranes were freeze-dried and the dried membranes were used for experiments.

2.3. Characterization

2.3.1. Microstructure characterization

Using a scanning electron microscope (SEM, S-4800, Hitachi, Japan), the prepared membrane's surface and cross-sectional morphology were examined. After drying, the membrane was trimmed to the proper size and fixed on the SEM sample holder using conductive adhesive. Prior to scanning, the sample holder was placed in a sputter coater, and the membrane was coated with gold for 40 s to enhance its conductivity.

2.3.2. Pore size measurement

A pore size distribution analyzer was used to determine the average pore size (GaoQ-PSMA-10, Nanjing Gaoqian Functional Materials Co., Ltd., China). The membrane sample was immersed in GQ-16 wetting solution (surface tension of 16 g·s^{-2}) for 12 h to ensure complete wetting of the membrane pores. In the test module, parameters such as operating pressure, maximum gas flow, and surface tension of the wetting solution were set in the software before starting the test. Once the test had been completed, the software's built-in program was used to calculate data mean the average pore size and the pore size distribution.

2.3.3. Porosity measurement

In this experiment, the gravimetric approach was used to measure the membrane's porosity. The membrane was first dried completely, cut to a specific size, and weighed using a balance, with its mass recorded as m_0. The sample was then immersed in kerosene for 24 h to ensure full wetting. Afterward, the sample was removed and only the kerosene that was still inside the membrane pores remained after the surface kerosene was carefully removed. The sample was weighed again, with its new mass recorded as m_1. The following formula was then used to determine the membrane's porosity:

$$\varepsilon = \frac{\frac{m_1 - m_0}{\rho_k}}{\frac{m_1 - m_0}{\rho_k} + \frac{m_0}{\rho_{mix}}} \times 100\% \quad (1)$$

$$\rho_{mix} = \frac{\omega_{PVDF} + \omega_{PVP} + \omega_{PEG}}{\frac{\omega_{PVDF}}{\rho_{PVDF}} + \frac{\omega_{PVP}}{\rho_{PVP}} + \frac{\omega_{PEG}}{\rho_{PEG}}} \quad (2)$$

where, ε represents the porosity of the membrane, %; m_1 represents the membrane's mass soaked in kerosene, g; m_0 represents the dry membrane's mass, g; ρ_{PVDF}, ρ_{PVP}, ρ_{PEG} represent the density of PVDF, PVP, PEG (1.78, 1.20, 1.13 g·cm^{-3}); ρ_k denotes the kerosene's density (0.81 g·cm^{-3}). ω_{PVDF}, ω_{PVP}, ω_{PRG} stand for the ratio of PVDF, PVP, PEG.

2.3.4. Contact angle determination

The surface contact angle of the membrane was measured using a contact angle goniometer (DropMeterA-100, Ningbo Hai shumai Testing Technology Co., Ltd., China). The sample was cut from the dried flat sheet membrane and affixed to a glass slide. A microsyringe was used to deposit a precise amount of water

droplets onto the room-temperature membrane surface. A computer was used to record the change in angle of contact between the membrane and the droplet interface over time. To minimize experimental error, each sample was tested three times.

2.3.5. Determination of mechanical properties

Mechanical characteristics of PVDF membrane were evaluated by two indicators: fracturing strength and elongation at break. In this experiment, an Edberg digital display tension meter (HLD1000, Zhejiang Ledibu Co., Ltd., China) was used for the measurements. First, a sample measuring 5 cm × 1 cm was cut from a flat sheet membrane utilizing a Japanese mould for knives. A thickness gauge was used to determine the sample's thickness (CF30559, Deqing Shengtaixin Electronic Technology Co., Ltd, China) before testing. After that, the sample was fastened at both ends, the tension meter was zeroed, and it was stretched at 25 °C at a steady rate of 5 mm·min^{-1}. The sample length and tension data were recorded at the moment the tension meter registered a value. The following formulas were used to determine the membrane's fracturing strength and elongation at break:

$$\theta = \frac{L_2 - L_1}{L_1} \times 100\% \tag{3}$$

$$\sigma = \frac{F}{A} \tag{4}$$

In Eqs. (3) and (4), θ represents the elongation at break of the membrane, %; L_1 represents the initial length of the membrane, m; L_2 represents the instantaneous length at the point of the membrane breakage, m; F represents the tensile force at fracture, N; σ represents the membrane's breaking strength, MPa; A represents the membrane area, m^2.

2.3.6. X-ray diffractometer analysis

An X-ray diffractometer (XRD, Miniflex600, Philosophy, Japan) with a Cu target was used to determine the crystal structure and type of the prepared membrane. The test conditions were as follows: tube current of 15 mA, acceleration voltage of 40 kV, angle range of 5° to 30°, and scanning speed of 5(°)·min^{-1}.

2.3.7. Fourier transform infrared spectrometer analysis

Using a Fourier transform infrared spectrometer (FT-IR, Nicolet 8700, Thermo Scientific, USA), the functional groups in the prepared membrane were examined. On the sample stage, a membrane segment of a particular size was scanned 32 times in attenuated total reflection (ATR) mode. The resolution was set to 4 cm^{-1}, and the wavenumber range for the test was set between 500 and 4000 cm^{-1}.

2.3.8. Zeta potential test

The surface charge of the membrane was measured using a zeta potential analyzer (Sur PASS, Anton Paar, Austria). Prior to testing, ensure the membrane is dry and clean the equipment with deionized water. 0.015 g of potassium chloride (KCl) was dissolved in 250 ml of deionized water to create an electrolyte solution. 0.1 mol·L^{-1} hydrochloric acid (HCl) and sodium hydroxide (NaOH) were used to modify the pH of the solution in order to evaluate the flow potential.

2.4. Blood compatibility test

2.4.1. pH test of membrane extract

A pH meter was used to measure the membrane extract's pH. Before testing, the membrane was dried, and a buffer solution was used to calibrate the pH meter. The membrane was trimmed to a certain weight and submerged in distilled water in a beaker, maintaining a mass ratio of 1:100 (membrane to water). After that, the beaker was submerged in a water bath with a constant temperature of 37 °C ± 1 °C. After 2 h, the extract was poured out, and its pH was measured. Once the pH reading stabilized, the value was recorded. Each sample was tested for three times, and the results were averaged.

2.4.2. UV absorbance test of membrane extract

The membrane extract was prepared according to the method described in Section 2.4.1 and placed in a colorimetric dish. Following the guidelines of Part 5.7 of GB/T14233.1—2022, the maximum absorbance value of the liquid in the wavelength range of 250–320 nm was measured using an ultraviolet–visible spectrophotometer (UV–Vis, UV-26001, Shimadzu, Japan). Distilled water was used as a blank control, with an absorbance value of 0 within the measured wavelength range.

2.4.3. Hemolysis rate test

According to the standard 'Medical infusion, blood transfusion, injection equipment testing methods, Part II: Biological test methods', the hemolysis rate of the material must meet the requirements specified in ISO 10993 and GB/T 16886. In general, a hemolysis rate of less than 5% indicates that the material has promising blood compatibility. The specific experimental steps are as follows:

(1) A 4:5 blood to normal saline ratio was used to dilute the blood.
(2) Ten milliliters of regular saline were combined with 200 μm of the diluted blood, then the cut membrane was immersed into the solution. The mixture was incubated on a shaker at 37 °C for 60 min.
(3) For 5 min, the solution was centrifuged at 1000 r·min^{-1}. A spectrophotometer was used to measure the absorbance of the supernatant at 540 nm after it had been collected.
(4) The positive control was diluted blood with purified water, and the negative control was diluted blood with normal saline. Eq. (5) was used to compute the hemolysis rate.

$$\text{Hemolysis rate} = (\text{Absorbance of a sample} - \text{Negative control absorbance})/(\text{Negative control absorbance} - \text{Positive control absorbance}) \times 100\% \tag{5}$$

2.4.4. Blood clotting time test

The clotting time test evaluates three parameters: clotting time (CT), activated partial thromboplastin time (APTT), and prothrombin time (PT). For the CT test, a sample cut to 6.0 cm × 1.5 cm was fixed onto a clean slide, 0.2 ml of fresh blood was applied to the sample surface, and the blood coagulation time was recorded. Each sample group was tested for three times. For APTT and PT tests, a membrane with area of 1.0 cm^2 was placed in anticoagulated blood and incubated at 37 °C for 5 min. A semi-automatic coagulation analyzer was used to determine APTT and PT values, with each group tested for three times.

2.4.5. Static protein adsorption capacity test

The membrane's ability to adsorb static proteins was assessed using BSA. The method involved staining the sample using a BCA protein assay kit and measuring the absorbance of the stained solution at a specific wavelength using a microplate reader. The

protein adsorption capacity was then calculated against the BSA standard curve. The detailed experimental procedure is as follows:

(1) BSA standard solution preparation: A BSA solution with a concentration of 0.5 g·L^{-1} was made using phosphate buffer solution (PBS). After serial dilutions, four additional BSA solutions with concentrations of 0.1, 0.2, 0.3, and 0.4 g·L^{-1} were prepared. These five concentrations were used to generate a standard curve.
(2) Preparation of BCA working solution: Using a ratio of BCA reagent A: B = 50:1, the BCA working solution was made based on the number of samples.
(3) Protein adsorption experiment: A 24-well plate was filled with 2 ml of the 0.5 g·L^{-1} BSA solution. The plate was incubated on a shaker at 37 °C for 2 h after a membrane measuring 1.0 cm^2 was submerged in the BSA solution.
(4) Determination of protein adsorption capacity: After incubation, 25 μl of BSA solution was transferred from the 24-well plate to a 96-well plate. The 96-well plate was then filled with 200 μl of the BCA working solution. For 30 min, the plate was incubated at 37 °C on a shaker. A microplate reader was used to measure the absorbance at 562 nm, and the BSA standard curve was used to calculate the protein concentration in the solution.

2.4.6. Determination of WBC removal rate

The efficiency of WBC removal during blood filtration can be calculated by comparing the number of WBCs before and after filtration. A sample of anticoagulated blood was mixed thoroughly and counted using an automated blood cell counter, which provides the initial WBC count before filtration. Since the WBC count in the filtered blood was significantly lower than the detection limit of the blood cell counter (10^9 L^{-1}), the manual counting method was employed for the post-filtration measurement. The procedure for manually counting WBCs is illustrated in Fig. 2.

First, the blood cell counting plate and glass cover plate with a 70% ethanol solution were cleaned before counting. After that, 0.38 ml of WBC diluent and 20 μl of blood sample were added into the test tube, and the two were thoroughly mixed to make WBC suspension for use. A period was stood for until the RBCs were completely destroyed and the suspension with WBC was added to the counting pool. After standing for 2–3 min, the WBCs in the four large squares at the four corners of the counting plate were counted by the principle of "recording on, not recording on the left, not recording on the right" with the low-power microscope, that is, the number of WBCs in the filtered blood. The calculation formula of the number of WBCs after filtration and the calculation formula of the specific WBC removal rate are as follows:

$$n_{w2} = \frac{N}{\text{counted surface} \times \text{chamber depth} \times \text{dilution}} \times 10^6 \quad (6)$$

$$\eta_w = \frac{n_{w1} - n_{w2}}{n_{w1}} \times 100\% \quad (7)$$

In Eq. (6), n_{w2} represents the quantity of WBCs in blood after filtration, cells·L^{-1}. N represents the overall quantity of WBCs in the four large squares, cells. In Eq. (7), η_w represents the WBC removal rate, %. n_{w1} represents the quantity of WBCs in the blood before filtration, cells·L^{-1}.

2.4.7. RBC and platelet recovery rates determination

The recovery rates of RBCs and PLTs during blood filtration refer to the percentage of RBCs and PLTs remaining after filtration compared with the initial count before filtration. Both pre- and post-filtration counts can be directly measured using an auto-

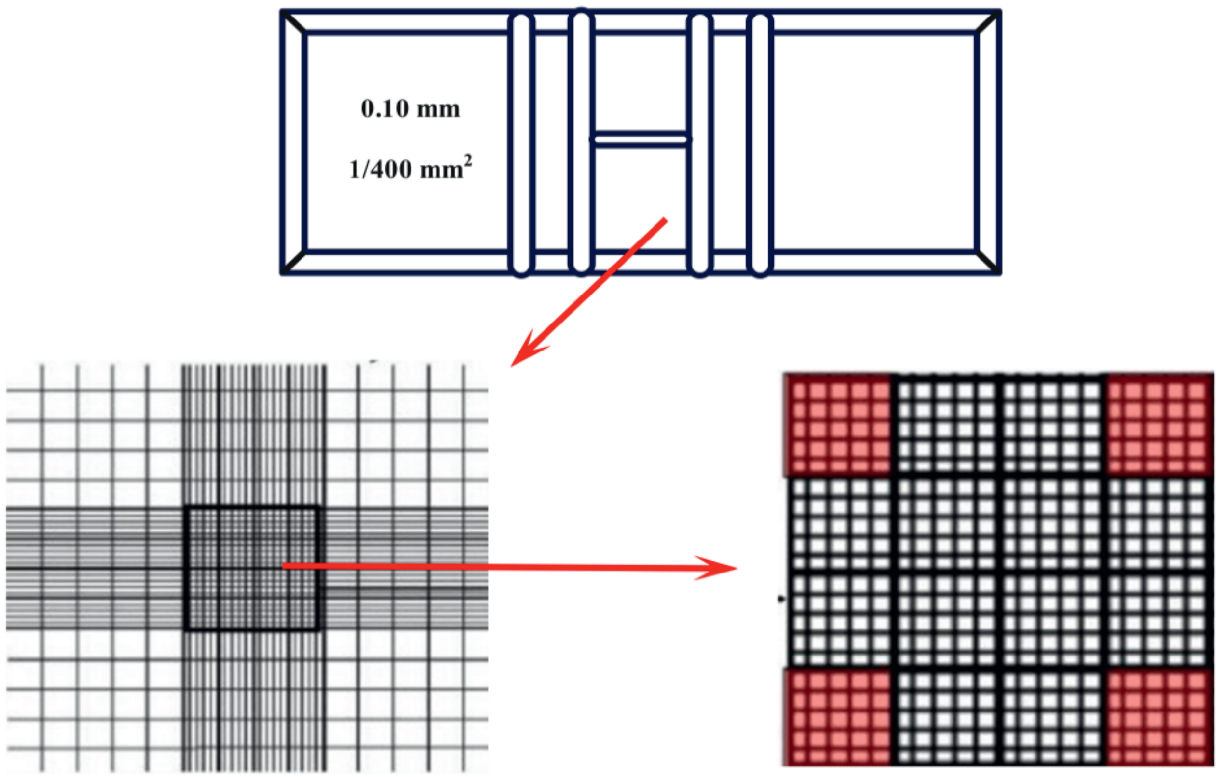

Fig. 2. The procedure for manually counting white blood cells.

mated blood cell counter. The specific equation for calculating the recovery rate is provided below.

$$\eta_r = \frac{n_{r2}}{n_{r1}} \times 100\% \quad (8)$$

In Eq. (8), η_r represents the recovery rate of RBCs or PLTs, %. n_{r1} denotes the number of RBCs or PLTs in the blood before filtration, cells·L^{-1}. n_{r2} represents the number of RBCs or PLTs in the blood after filtration, cells·L^{-1}.

3. Results and Discussion

3.1. Physical properties of PVDF/PVP/PEG blend membrane

During the preparation of polymeric membranes using VIPS process, the concentration of polymers significantly affects the pore size and microscopic morphology. When the ratio of PVP K90 and PEG 600 additives in the cast film solution is small, the polymer solution undergoes a similar phase separation process. However, when the ratio of PVP to PEG is large, the viscosity of the cast film solution increases due to the much larger molecular weight of PVP K90 (Mw = 360000 Da) compared to PEG 600 (Mw = 600 Da). The viscosity of the casting solution gradually increases with the addition of PVP K90. The thermodynamic instability of the solvent in the polymer solution increases during interaction with the non-solvent, showing a transient delamination mechanism. The addition of PVP K90 also promotes the formation of large pores during membrane preparation. Therefore, for investigating the impact of PVDF concentration on the pore size and functionality of the produced membranes, an additive ratio of 8:2 was chosen for PVP K90 to PEG 600. The specific composition of the casting solution and the membrane preparation conditions are shown in Table 1, where M1, M2, and M3 represent membranes prepared with different PVDF concentrations, respectively.

Fig. 3 demonstrates the microstructure of the membranes made with varying amounts of PVDF. The figure illustrates how the membrane's surface pore density rose in tandem with the PVDF concentration, resulting in a more evenly distributed distribution of surface pores. However, the morphology of these surface pores remained irregular. Additionally, the membrane's cross section changed from having a cellular to a nodular form, enhancing the connectivity among membrane pores. This phenomenon can be attributed to changes in polymer concentration affecting the phase separation process. With higher polymer (PVDF) concentrations, the casting solution's viscosity rose, increasing the entanglement between polymer molecular chains. This results in a decreased migration rate of polymer molecular chains and a slowdown in the diffusion rates of solvent and non-solvent in the polymer solution, thereby influencing the kinetics of the phase separation process.

Fig. 4(a), (b) and (c) illustrate the average pore size, pore size precents and the porosity of membranes made with three distinct amounts of PVDF. The figures indicate that as the PVDF concentration increased, the membrane's average pore size shrank at high PVDF concentrations, the membranes exhibited smaller pore sizes and narrower distributions. Conversely, at low concentrations, the membranes exhibited larger pore sizes and wider distributions, while maintaining an overall porosity of approximately 80%. This phenomenon arises from the higher viscosity of the casting solution at elevated PVDF concentrations, which increases polymer chain entanglement, thereby hindering solvent (DMAc) evaporation and non-solvent (water vapor) penetration. The delayed phase separation process favors the formation of dense structures over microporous architectures generated by rapid phase separation.

The membranes' tensile strength marginally increased as the PVDF concentration rose, as seen in Fig. 5(a), while the elongation at break remained relatively mass constant at around 15%. This is primarily because at lower PVDF concentrations, the membrane had larger pore sizes and higher porosity, leading to weaker interactions between the polymer molecular chains and thus lower mechanical strength. Conversely, at higher PVDF concentrations, the opposite effect was observed, with smaller pore sizes and lower porosity resulting in stronger interactions between the polymer chains and the increased mechanical strength.

The surface roughness of the membranes prepared with different PVDF concentrations is presented in Fig. 5(b). As the PVDF concentration in the casting solution increased, the surface roughness of the membrane decreased from 70 nm to 31.6 nm. Blending PVDF with hydrophilic polymers (PEG/PVP) creates rough surfaces rich in hydrophilic sites, reducing the intrinsic contact angle. The Wenzel model predicts that surface roughness amplifies hydrophilicity: for inherently hydrophilic materials, micro/nanostructures (*e.g.*, grooves, pores) enhance liquid–solid contact area and wetting pathways, further decreasing the apparent contact angle.

The PVDF concentration had a considerable impact on the membrane's contact angle, as observed in Fig. 5(c). The membrane's contact angle tends to grow as the concentration of polymers increases. Strongly polar C–F bonds are produced by the fluorine atoms' high electronegativity in PVDF, leading to dense molecular packing and reduced surface energy. Since lower surface energy correlates with higher hydrophobicity, PVDF inherently exhibits strong hydrophobicity. Increasing PVDF concentration enhances membrane hydrophobicity by elevating the density of C–F hydrophobic groups on both the surface and interior. Pramono *et al.* [33] investigated how PVDF concentration affected membrane characteristics and discovered that PVDF is naturally hydrophobic, therefore, higher PVDF concentrations result in lower interactions between the membrane and water.

Fig. 5(d) depicts the zeta potential of the membranes prepared with varying PVDF concentrations. Membranes M1, M2, and M3 each exhibited negative charges, with their magnitudes decreasing sequentially in the order M1 > M2 > M3. At a pH value of 7, the corresponding zeta potential values for the three membranes were −4.82, −10.27, and −10.68 mV, respectively. This negative charge on the membrane surface exerted a repulsive effect on WBCs.

3.2. Chemical properties of PVDF/PVP/PEG blend membranes

The XRD patterns of the blended membranes made with three distinct PVDF ratios are displayed in Fig. 6(a). The figure

Table 1
Casting solution mass compositions and conditions of membranes preparation.

Number	PVDF/%	PVP K90/%	PEG 600/%	DMAc/%	Vapor-initiated time/min
M1	14	8	2	76	5
M2	16	8	2	74	5
M3	18	8	2	72	5

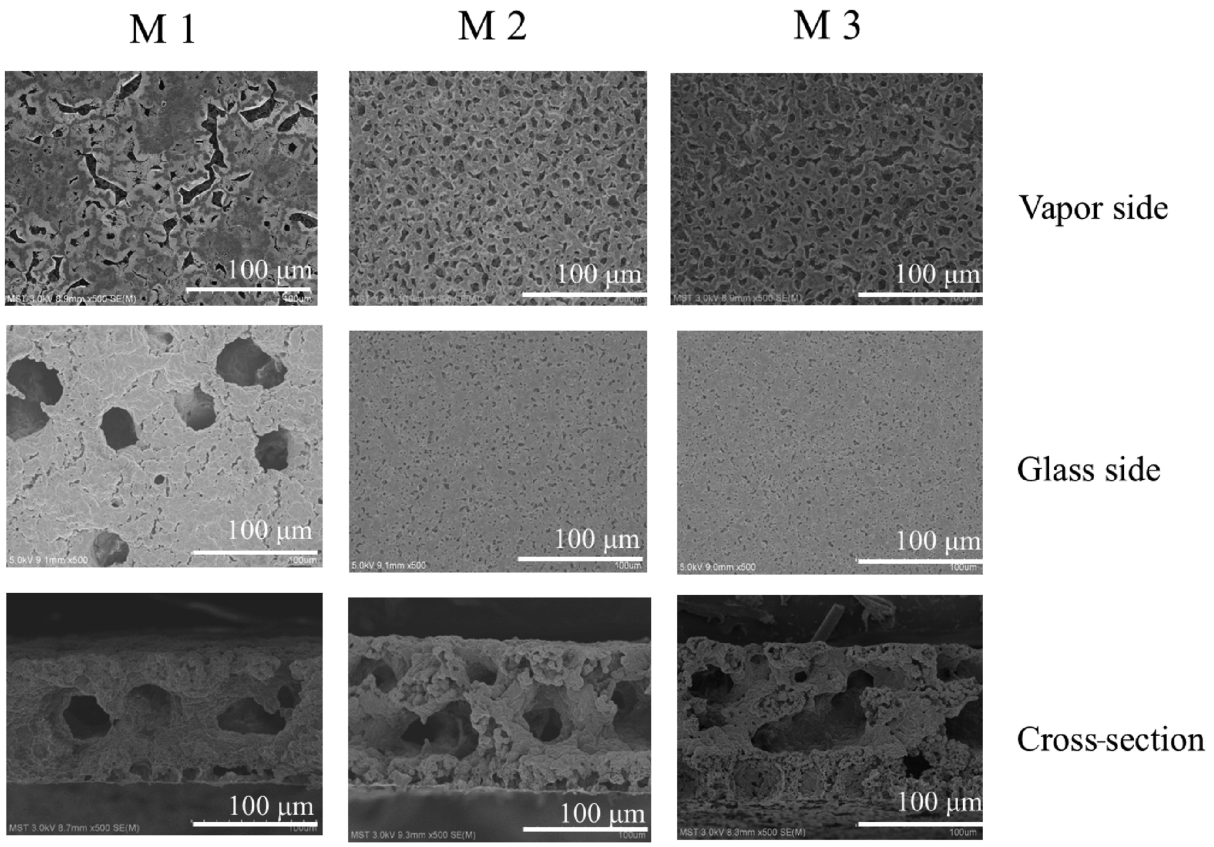

Fig. 3. SEM images of the membranes made with varying amounts of PVDF.

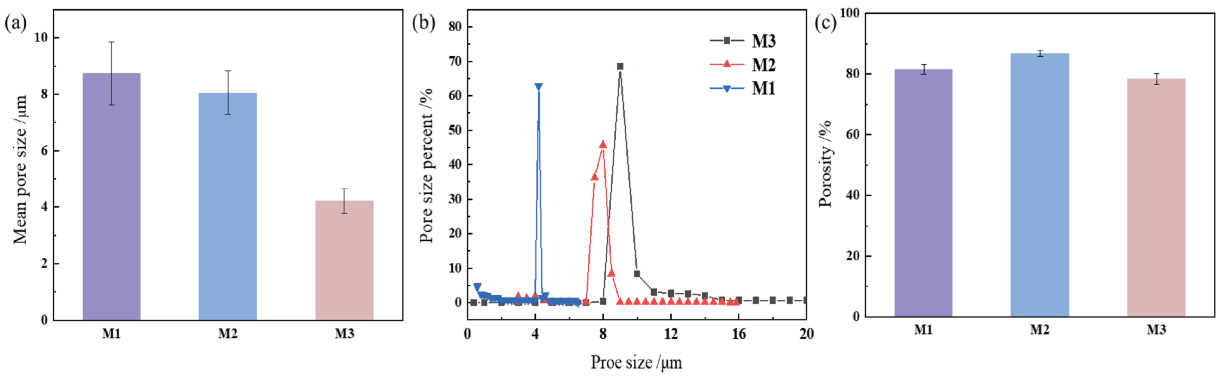

Fig. 4. (a) Average pore size, (b) pore size precents, and (c) porosity of membranes made with distinct amounts of PVDF.

reveals characteristic peaks around 18.3°(α), 20.1°(β), and 26.56°(α), indicating that membranes M1, M2, and M3 contained a combination of α and β phases, with the α phase predominating.

Fig. 6(b) displays the membranes' FT-IR spectra made using varying PVDF proportions. The spectra indicate that membranes M1, M2, and M3 exhibit distinct infrared absorption peaks for C═O groups at 1675 cm^{-1}, and −C−N− stretching vibration peaks at 1424 cm^{-1}, confirming the successful blending of PVP K90 with the PVDF polymer in the membrane formation process. Additionally, characteristic peaks at 762, 795, 876, 1070, and 1179 cm^{-1} are consistent with α phase PVDF, while peaks at 840 and 1404 cm^{-1} can be attributed to β phase PVDF. This suggests that the prepared PVDF membranes consisted of a mixture of α and β phases. Previous studies have reported that α-phase PVDF exhibits lower protein adsorption compared to β-phase PVDF. The β-phase PVDF, due to the opposite charges on both sides of its carbon chain, possesses polarity, which promotes protein adsorption on its surface and is detrimental to blood filtration [34].

3.3. Blood compatibility of PVDF/PVP/PEG blend membranes

3.3.1. pH value

The pH level of human blood typically remains stable between 7.3 and 7.5, and deviations from this range can be detrimental to human health. To evaluate the handmade membranes M1, M2, and M3 for chemical safety, the pH of the solutions before and after membrane

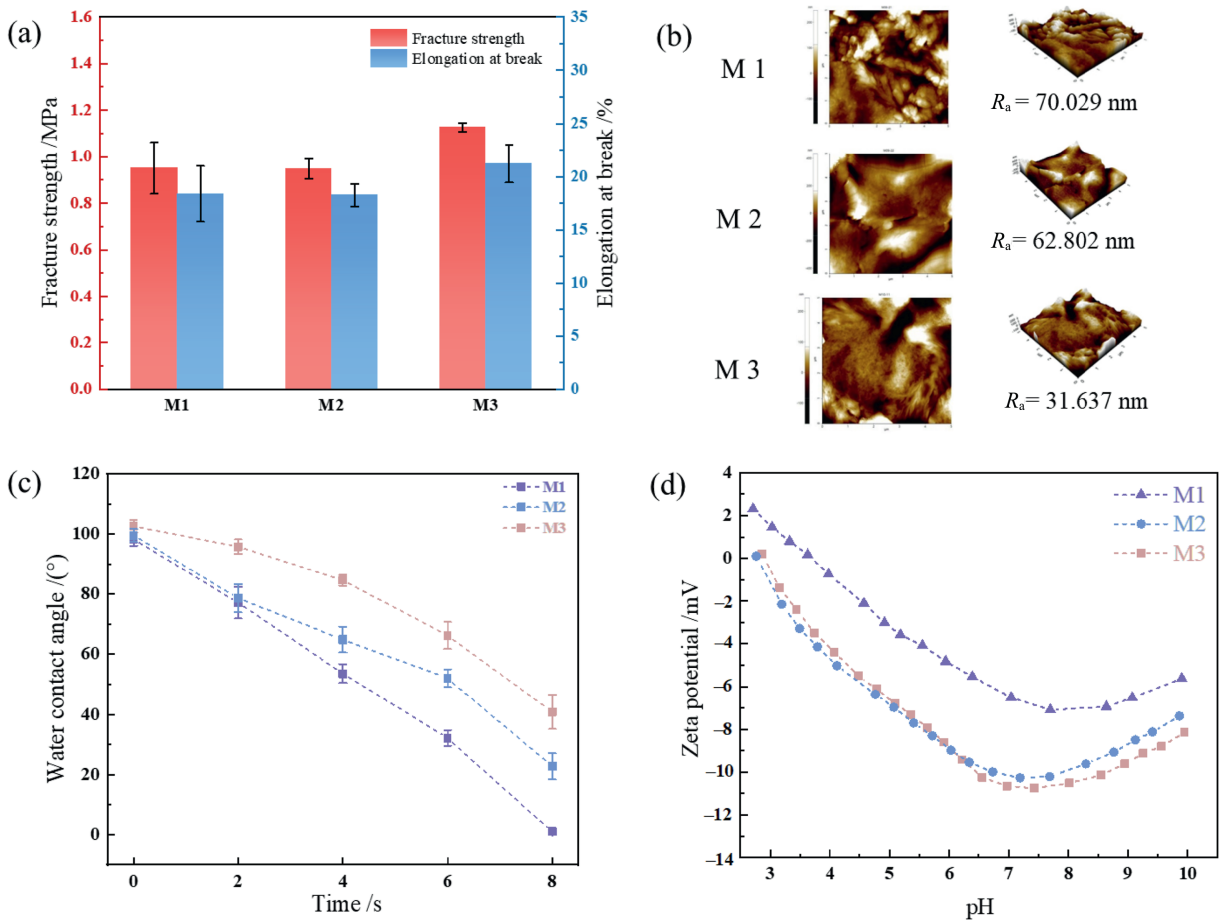

Fig. 5. (a) Mechanical strength and elongation at break, (b) roughness, (c) contact angle, and (d) zeta potential of the membranes prepared with different PVDF concentrations.

immersion was measured. These solutions were prepared following the experimental procedures outlined in Section 2.4.1.

Fig. 7(a) illustrates the pH changes of the solutions before and after membrane immersion. The results indicate that the pH differences between the extract solutions and the original solutions for the three homemade membranes range from 0.15 to 0.26. These differences are significantly lower than the 1.5 threshold specified by the national standard GB/T14233.1 “Medical Infusion, Blood Transfusion, Injection Equipment Test Method Part I: Method of Chemical Analysis”. Consequently, the minimal pH changes observed before and after membrane immersion demonstrate that the material meets the application requirements.

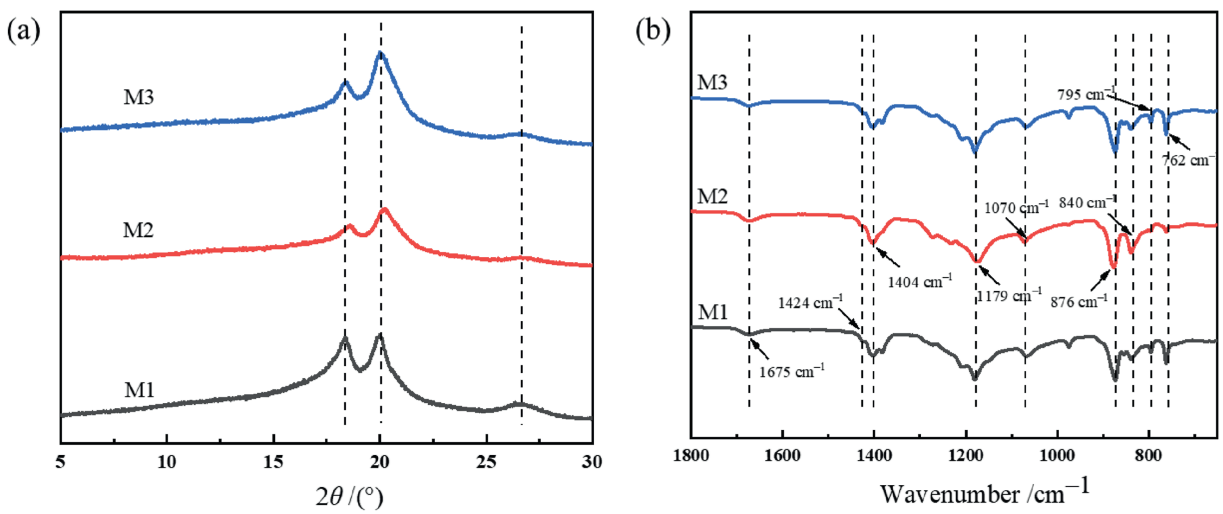

Fig. 6. (a) XRD patterns and (b) FT-IR spectra of the blend membranes.

3.3.2. UV absorbance

The UV absorbance of the extracts from self-made membranes M1, M2, and M3 is shown in Fig. 7(b). It ranged from 0.075 to 0.125, which are all lower than the 0.3 threshold specified by the national standard GB/T14233.1 ″Medical Infusion, Blood Transfusion, Injection Equipment Test Method Part I: Method of Chemical Analysis" for blood filtration materials in the wavelength range of 250–320 nm. Therefore, in terms of organic matter content, the self-made membranes meet the required standards for use.

3.3.3. Protein adsorption

The interaction between proteins and material surfaces has been a central focus in the field of biocompatibility research. When a liquid containing soluble proteins, such as blood or tissue fluid, comes into contact with a material's surface, the proteins in the liquid first rapidly adhere to the material's surface. Following this, cells make indirect contact with the material's surface through the protein molecular layer that has formed. Hence, if the adhesion behavior or state of the proteins on the surface of the material can be modified to some extent, it becomes possible to control the interaction between the cells and the protein molecular layer, thereby influencing the biological response of the cells.

The findings displayed in Fig. 7(c) reveal that the protein adsorption capacity of membranes M1, M2, and M3 increased slightly in sequence. This could be attributed to the increased surface roughness and initial contact angle of M2 and M3 relative to M1, leading to a marginally higher protein adsorption capacity. However, the overall protein adsorption capacity of these membranes remained relatively low, at approximately 30–40 $\mu g \cdot cm^{-2}$. Notably, compared to the commercial membrane M0, the protein adsorption capacity of M1 had decreased to some extent.

3.3.4. Hemolysis rate

Hemolysis refers to the rupture and dissolution of RBCs upon encountering exogenous substances. This experiment aims to assess the extent of damage to RBCs caused by exogenous substances, such as cholate, present in homemade membranes. Testing the hemolysis rate of these membranes can directly indicate whether they release any harmful substances that damage blood cells upon contact. A high hemolysis rate suggests that the membrane alters the physical and blood cells' chemical characteristics when in usage, which can result in hemolysis and other negative consequences, thereby posing a threat to the life and health of the blood recipient. Section 2.4.3 outlines the procedure used to measure the membranes' hemolysis rate.

Fig. 7(d) illustrates the hemolysis rates of the homemade membranes M1, M2, and M3. It ranged from 2% to 3%. It is noteworthy that M1's hemolysis rate is lower than that of the commercial membrane M0. All the membranes meet the ISO 10993 and GB/T16886 standards, which stipulate that the hemolysis rate of blood-contacting materials should be less than 5%. Consequently, these materials do not cause damage to RBCs upon contact with blood, confirming their safety.

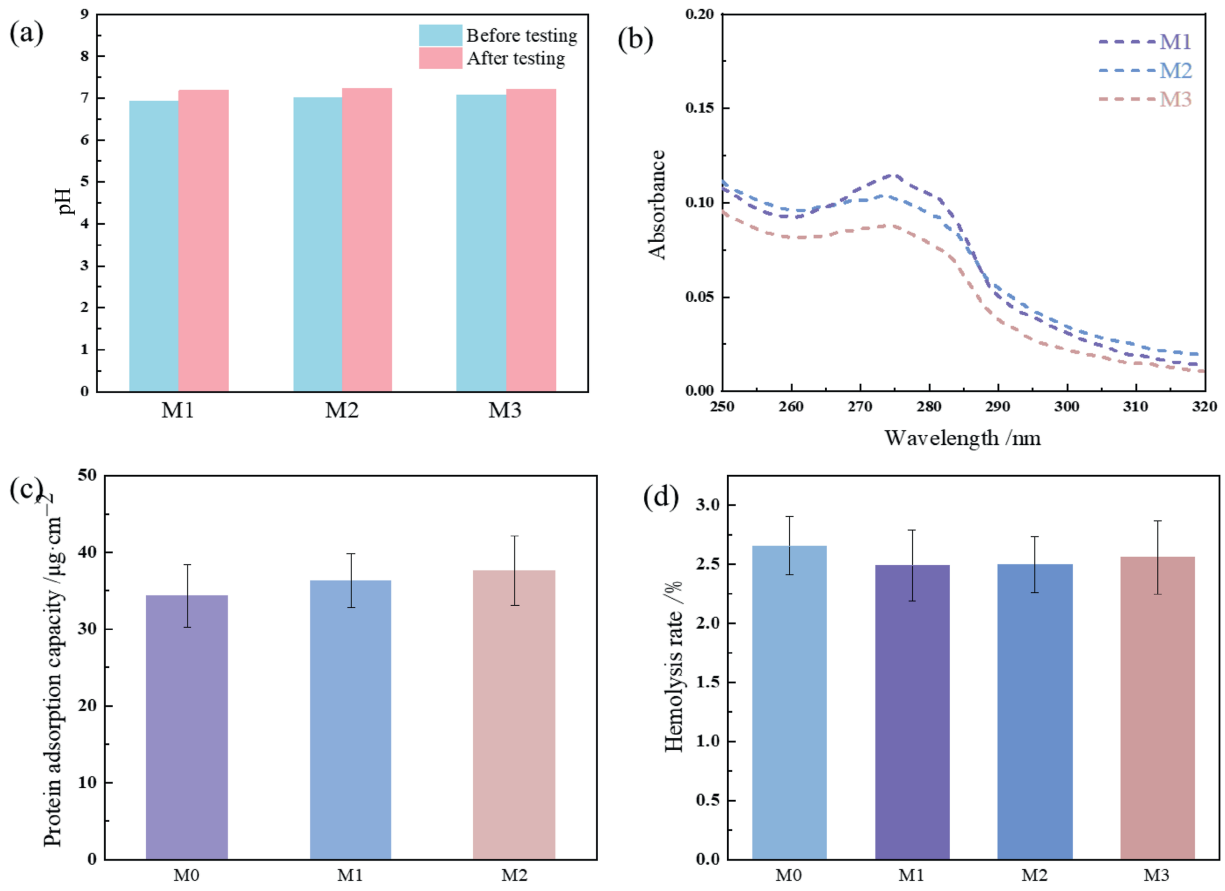

Fig. 7. PVDF/PVP/PEG blend membranes: (a) pH, (b) UV absorbance, (c) protein adsorption, (d) hemolysis rate.

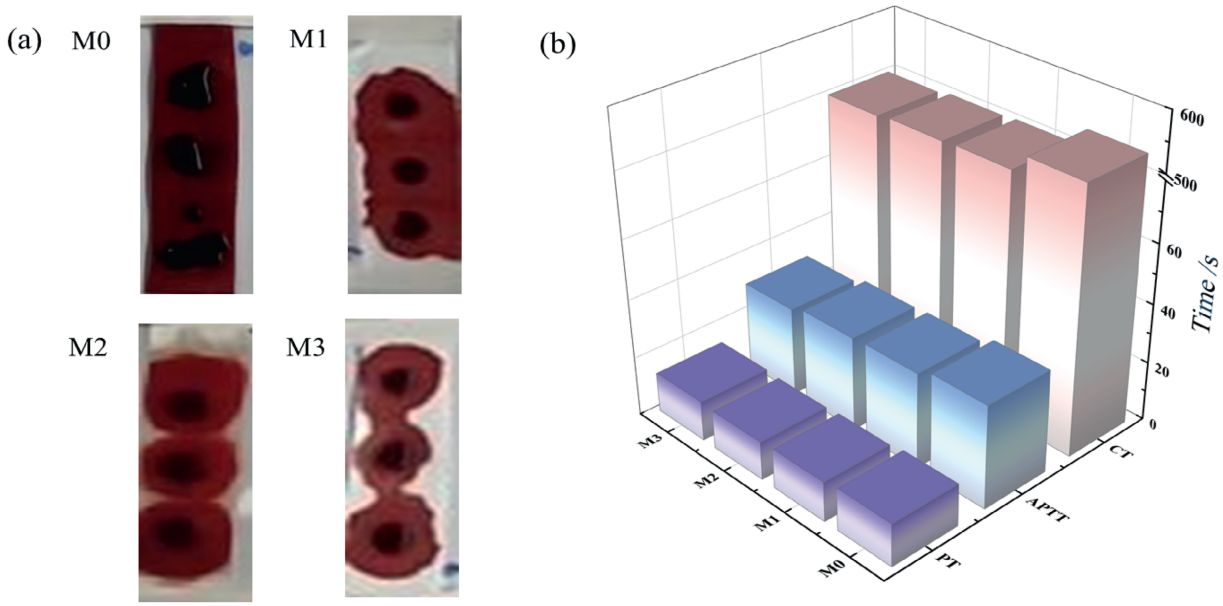

Fig. 8. (a) CT test process and (b) CT, APTT and PT.

3.3.5. Coagulation time

The CT, APTT, and PT test results for the homemade membranes M1, M2, and M3 are displayed in Fig. 8(a) and (b), along with comparisons to the commercial membrane M0. The results indicate that when the membranes came into contact with blood, the CT and APTT values decrease compared to the original blood. This decrease is attributed to the release of foreign substances into the blood, altering the coagulation state. In contrast, the PT values do not show significant changes, suggesting that these membranes do not have a noticeable inhibitory effect on exogenous coagulation.

3.4. Whole blood filtration

To evaluate the filtration performance of the PVDF/PVP/PEG blend membranes, whole blood filtration tests were conducted. Membrane M1 was chosen due to its suitable pore size, hydrophilicity, biocompatibility, and acceptable hemolysis rate, and a single filtration layer was used. The effect of different filtration temperatures (body temperature, room temperature, and low temperature) on the blood filtration performance was investigated.

Fig. 9 illustrates how the filtration temperature affects the PVDF/PVP mix membrane's (M1) ability to remove leukocytes. The results indicate that as the filtration temperature decreased, the concentration of WBCs in the filtered blood continued to drop, and the removal rate of WBCs gradually increased—from 9.79×10^8 L^{-1} at 37 °C to 5.10×10^8 L^{-1}, and from 84.73% to 92.04%. Although the recovery rate of RBCs decreased, it remained above 90%. This may be attributed to the fact that the deformability of blood cells was influenced by blood temperature. At lower blood temperatures, the deformability of blood cells was reduced, increasing the likelihood that WBCs will be trapped inside the membrane's pores and on its surface. However, this also increased the difficulty for RBCs, which had poor deformability at low temperatures, to pass through the filter material.

The effect of the quantity of filtration layers on the PVDF leukocyte removal membrane's filtration performance is shown in Fig. 10. The data show that for membrane M1, the concentration of WBCs in the filtered blood decreased significantly as the number of filtration layers increased. However, this led to a decrease in the RBC recovery rate as well. Notably, the removal rate of WBCs reached 98.36%. Compared to blood before filtration, the concentration of WBCs was reduced by an order of magnitude, while the recovery rate of RBCs remained above 85%.

Once the number of filtration layers exceeds one, blood fails to permeate membrane M3, rendering it ineffective for blood

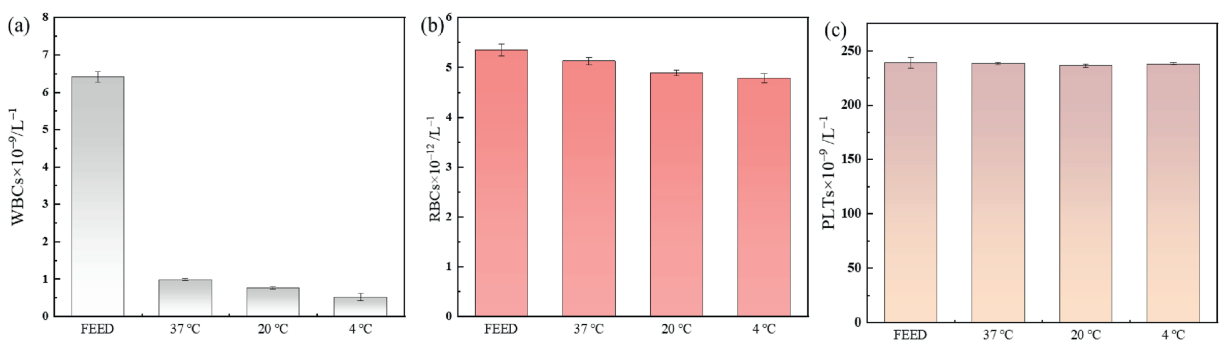

Fig. 9. Blood filtration performance of the membrane at different temperatures: (a) white blood cells, (b) red blood cells, (c) platelets.

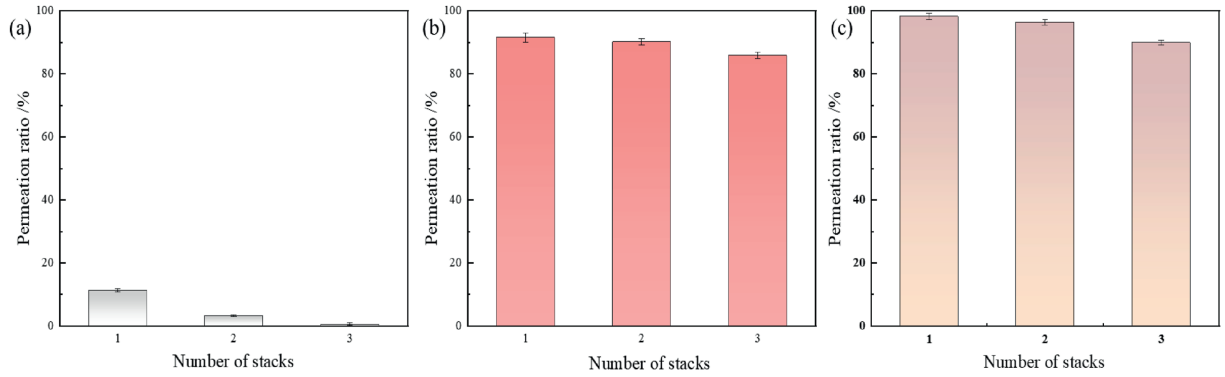

Fig. 10. Blood filtration performances of the membrane with different numbers of stacked layers: (a) white blood cells (b) red blood cells (c) platelets.

filtration. Similarly, membrane M2 cannot facilitate blood passage under more than two filtration layers. This can be explained by two main factors: Increasing the number of filtration layers altered the hydrodynamic pathway of blood. This redesign generated tortuous microchannels within the filter matrix, which enhanced leukocyte retention efficacy. However, erythrocyte transit was simultaneously hindered due to elevated shear stress and steric hindrance. Second, the stacking of multiple filter layers reduced the average pore size [35]. The presence of smaller pores, much smaller than the diameter of blood cells, led to the clogging of these pores by blood cells, preventing smooth blood flow.

4. Conclusions

This study demonstrates that the blood compatibility and filtration efficacy of PVDF-based membranes are critically governed by polymer concentration, filtration architecture, and operational parameters. The 14% (mass) PVDF membrane exhibited superior hemocompatibility with minimal hemolysis (<5%) and low protein adsorption, outperforming commercial counterparts. Key mechanistic insights revealed an inherent trade-off between leukocyte removal efficiency and erythrocyte recovery rate: reducing pore size enhanced leukocyte retention but compromised erythrocyte passage, particularly in single-layer configurations. Multilayer filtration amplified leukocyte exclusion, yet excessive layering (≥2 layers) with higher PVDF mass concentrations (16% to 18%) led to pore size constriction, drastically reducing erythrocyte recovery. Optimal performance was achieved with a triple-layer 14% (mass) PVDF membrane at 4 °C, balancing a leukocyte removal rate of 98.36% with >85% erythrocyte recovery. These findings offered a highly efficient solution for blood cell separation, balancing both high white blood cell removal and satisfactory red blood cell recovery.

CRediT Authorship Contribution Statement

Ziqi Jin: Writing – original draft, Investigation, Formal analysis. Shuang Yao: Writing – review & editing, Investigation, Formal analysis. Liang Li: Validation, Investigation. Siyuan Sun: Validation, Investigation. Yue Zhou: Validation, Investigation. Jie Zhou: Validation, Investigation. Zhaohui Wang: Writing – review & editing, Supervision, Methodology, Conceptualization. Zhaoliang Cui: Writing – review & editing, Supervision, Methodology, Conceptualization.

Declaration of Competing Interest

The authors declare that they have no known competing financial interests or personal relationships that could have appeared to influence the work reported in this paper.

Acknowledgements

The National Key Research and Development Program of China (2020YFC0862903), Supported by Jiangsu Future Membrane Technology Innovation Center (BM2021804), National Foreign Expert Program (H20240294).

References

[1] Y.J. Wang, Q. Rao, X.F. Li, Adverse transfusion reactions and what we can do, *Expert Rev. Hematol* 15 (8) (2022) 711–726.
[2] H. Meryman, J. Bross, R. Lebovitz, The preparation of leukocyte-poor red blood cells: a comparative study, *Transfusion* 20 (3) (1980) 285–292.
[3] G. Sirchia, A. Parravicini, P. Rebuild, L. Fattori, S. Milani, Evaluation of three procedures for the preparation of leukocyte-poor and leukocyte-free red blood cells for transfusion, *Vox Sang.* 38 (4) (1980) 197–204.
[4] M. Uda, S. Naito, K. Yamamoto, A. Ishii, T. Nishizaki, Optimal protocol for preparation of leukocyte-poor red cells with a blood cell processor, *Transfusion* 24 (2) (1984) 120–123.
[5] J.P. Crowley, P.H. Wade, C. Wish, C.R. Valeri, The purification of red cells for transfusion by freeze-preservation and washing V. red cell recovery and residual leukocytes after freeze-preservation with high concentrations of glycerol and washing in various systems, *Transfusion* 17 (1) (1977) 1–7.
[6] C. Weinstock, M. Schnaidt, Human leucocyte antigen sensitisation and its impact on transfusion practice, *Transfus. Med. Hemother.* 46 (5) (2019) 356–369.
[7] C.J.O. Bacal, J.W. Maina, H.H. Nandurkar, M. Khaleel, R. Guijt, Y. Chang, K.M. Dwyer, L.F. Dumée, Blood apheresis technologies—a critical review on challenges towards efficient blood separation and treatment, *Mater. Adv.* 2 (22) (2021) 7210–7236.
[8] S. Dzik, J. Aubuchon, L. Jeffries, S. Kleinman, C. Manno, M.F. Murphy, M.A. Popovsky, M. Sayers, L.E. Silberstein, S.J. Slichter, E.C. Vamvakas, Leukocyte reduction of blood components: public policy and new technology, *Transfus. Med. Rev.* 14 (1) (2000) 34–52.
[9] R.R. Sharma, N. Marwaha, Leukoreduced blood components: advantages and strategies for its implementation in developing countries, *Asian J. Transfus. Sci.* 4 (1) (2010) 3–8.
[10] U. Nobis, A.R. Pries, G.R. Cokelet, P. Gaehtgens, Radial distribution of white cells during blood flow in small tubes, *Microvasc. Res.* 29 (3) (1985) 295–304.
[11] A. Bruil, J.I. Sheppard, J. Feijen, I.A. Feuerstein, *In vitro* leukocyte adhesion to modified polyurethane surfaces: III. effect of flow, fluid medium, and platelets on PMN adhesion, *J. Biomater. Sci. Polym. Ed.* 5 (4) (1994) 263–277.
[12] C.A. Scotchford, C.P. Gilmore, E. Cooper, G.J. Leggett, S. Downes, Protein adsorption and human osteoblast-like cell attachment and growth on alkylthiol on gold self-assembled monolayers, *J. Biomed. Mater. Res.* 59 (1) (2002) 84–99.
[13] J.N. Barbosa, M.A. Barbosa, A.P. Aguas, Adhesion of human leukocytes to biomaterials: an *in vitro* study using alkanethiolate monolayers with different chemically functionalized surfaces, *J. Biomed. Mater. Res.* 65 (4) (2003) 429–434.
[14] A.S.G. Curtis, J.V. Forrester, P. Clark, Substrate hydroxylation and cell adhesion, *J. Cell Sci.* 86 (1) (1986) 9–24.
[15] J.H. Lee, J.W. Park, H.B. Lee, Cell adhesion and growth on polymer surfaces with hydroxyl groups preparedby water vapour plasma treatment, *Biomaterials* 12 (5) (1991) 443–448.
[16] C. Yang, K. Sun, J.X. Liu, H. Wang, Y. Cao, Zwitterionic sulfobetaine-modified non-woven fabric for blood filtration, *Polym. Int.* 59 (9) (2010) 1296–1302.
[17] A.S. Curtis, J.V. Forrester, C. McInnes, F. Lawrie, Adhesion of cells to polystyrene surfaces, *J. Cell Biol.* 97 (5) (1983) 1500–1506.
[18] D.R. Absolora, E.L. Snyder, Role of filter surface tension in the retention of cellular elements by microaggregate blood filters, *J. Dispers. Sci. Technol.* 6 (1) (1985) 37–53.

[19] P.V. Mayuri, A. Bhatt, R. Joseph, P. Ramesh, Effect of photografting 2-hydroxyethyl acrylate on the hemocompatibility of electrospun poly (ethylene-co-vinyl alcohol) fibroporous mats, *Mater. Sci. Eng. C Mater. Biol. Appl.* 60 (2016) 19–29.
[20] A.P. Marques, R.L. Reis, J.A. Hunt, The effect of starch-based biomaterials on leukocyte adhesion and activation *in vitro*, *J. Mater. Sci. Mater. Med.* 16 (11) (2005) 1029–1043.
[21] S.N. Rodrigues, I.C. Gonçalves, M.C.L. Martins, M.A. Barbosa, B.D. Ratner, Fibrinogen adsorption, platelet adhesion and activation on mixed hydroxyl-/methyl-terminated self-assembled monolayers, *Biomaterials* 27 (31) (2006) 5357–5367.
[22] X.P. Xiong, Y.G. Wang, C.T. Zhong, Preparation of an asymmetric membrane *via* vapor induced phase separation for membrane distillation, *Prog. Org. Coat.* 181 (2023) 107590.
[23] A. Venault, J.R. Wu, Y. Chang, P. Aimar, Fabricating hemocompatible bicontinuous PEGylated PVDF membranes *via* vapor-induced phase inversion, *J. Membr. Sci.* 470 (2014) 18–29.
[24] A. Venault, M.R.B. Ballad, Y.T. Huang, Y.H. Liu, C.-H. Kao, Y. Chang, Antifouling PVDF membrane prepared by VIPS for microalgae harvesting, *Chem. Eng. Sci.* 142 (2016) 97–111.
[25] J.S. Zhang, Y. Wu, M.S. Xia, Q.J. Yang, Q.Y. Xu, W.W. Feng, PVDF membrane with tea powder adhered for efficient separation of emulsified oil, *Kor. J. Chem. Eng.* 40 (10) (2023) 2376–2383.
[26] Q.D. Wu, A. Tiraferri, T. Li, W.C. Xie, H.Q. Chang, Y.H. Bai, B.C. Liu, Superwettable PVDF/PVDF-*g*-PEGMA ultrafiltration membranes, *ACS Omega* 5 (36) (2020) 23450–23459.
[27] L.C. Malucelli, I. Ozeri, M. Matos, W.L.E. Magalhães, M.A.S.C. Filho, M.S. Eisen, High-flux, porous and homogeneous PVDF/cellulose microfiltration membranes, *Cellulose* 29 (3) (2022) 1943–1953.
[28] M. Oliveira Filho, R. Mailler, V. Rocher, Y. Fayolle, C. Causserand, Comprehensive study of supported PVDF membrane ageing in MBR: a direct comparison between changes at bench scale and full scale, *Sep. Purif. Technol.* 279 (2021) 119695.
[29] C.B. Geng, F.B. Zhao, Q. Wang, S. Zheng, Y. Liu, H.Y. Niu, J.M. Zhang, H.X. Dong, Anti-biofouling property and anti-leaching investigation of modifier for PVDF ultrafiltration membrane by incorporating antibacterial graphene oxide derivatives, *J. Environ. Chem. Eng.* 10 (6) (2022) 108558.
[30] Y.X. Zhang, X.F. Duan, B.R. Tan, Y.C. Jiang, Y. Wang, T. Qi, PVDF microfiltration membranes modified with AgNPs/tannic acid for efficient separation of oil and water emulsions, *Colloids Surf. A Physicochem, Eng. Aspects* 644 (2022) 128844.
[31] M. Husain, R. Singh, B.S. Pabla, On 3D printing of PVDF composite- based sensors for biomedical applications, *Natl. Acad. Sci. Lett.* 47 (2) (2024) 147–152.
[32] A. Venault, Y.T. Chin, I. Maggay, C.C. Yeh, Y. Chang, Poly(vinylidene fluoride)/poly(styrene-co-acrylic acid) nanofibers as potential materials for blood separation, *J. Membr. Sci.* 641 (2022) 119881.
[33] E. Pramono, A.L. Simamora, C.L. Radiman, D. Wahyuningrum, Effects of PVDF concentration on the properties of PVDF membranes, *IOP Conf. Ser. Earth Environ. Sci.* 75 (1) (2017) 012027.
[34] J.Y. Miao, D.H. Reneker, M. Tsige, P.L. Taylor, Molecular dynamics simulations and morphology analysis of TEM imaged PVDF nanofibers, *Polymer* 125 (2017) 190–199.
[35] R. Pourbaghi, M. Zarrebini, D. Semnani, A. Pourazar, N. Akbari, R. Shamsfar, Evaluation of polyacrylonitrile electrospun nano-fibrous mats as leukocyte removal filter media, *J. Biomed. Mater. Res. B Appl. Biomater.* 106 (5) (2018) 1759–1769.